FINNISH METEOROLOGICAL INSTITUTE
CONTRIBUTIONS

No. 130

Data assimilation and numerical modelling of atmospheric composition

Julius Vira

Academic dissertation in physics

To be presented, with the permission of the Faculty of Science of the University of Helsinki, for public criticism in the auditorium "Brainstorm" of Finnish Meteorological Institute (Erik Palménin aukio 1, Helsinki) on February 23th, 2017 at 12 o'clock noon.

Finnish Meteorological Institute
Helsinki, 2017

Author's address: Julius Vira
Finnish Meteorological Institute
Atmospheric Composition Research
P.O. BOX 503
FI-00101 Helsinki, Finland
e-mail julius.vira@fmi.fi

Supervisor: Docent Mikhail Sofiev
Finnish Meteorological Institute

Reviewers: Docent Joakim Langner
Swedish Meteorological and Hydrological Institute

Professor Wouter Peters
Department of Meteorology and Air Quality
Wageningen University

Opponent: Dr. Adrian Simmons
European Centre for Medium-Range Weather Forecasts

Custos: Professor Veli-Matti Kerminen
Department of Physics
University of Helsinki

ISBN 978-952-336-011-2 (paperback)
ISSN 0782-6117
Erweko Oy
Helsinki 2017

ISBN 978-952-336-012-9 (pdf)
Helsingin yliopiston verkkojulkaisut
http://ethesis.helsinki.fi

FINNISH METEOROLOGICAL INSTITUTE

Published by
Finnish Meteorological Institute
P.O. Box 503
FI-00101 Helsinki, Finland

Series title, number and report code of publication
Finnish Meteorological Institute
Contributions 130, FMI-CONT-130

Date
February 2017

Author
Julius Vira

Title
Data assimilation and numerical modelling of atmospheric composition

Abstract

Atmospheric chemistry and transport models are used for a wide range of applications which include predicting dispersion of a hazardous pollutants, forecasting regional air quality, and modelling global distribution of aerosols and reactive gases. However, any such prediction is uncertain due to inaccuracies in input data, model parametrisations and lack of resolution. This thesis studies methods for integrating remote sensing and in-situ observations into atmospheric chemistry models with the aim of improving the predictions.

Techniques of data assimilation, originally developed for numerical weather prediction, are evaluated for improving regional-scale predictions in two forecast experiments, one targeting the photochemical pollutants ozone (O_3) and nitrogen dioxide (NO_2), the other targeting sulphur dioxide (SO_2). In both cases, assimilation of surface-based air quality monitoring data is found to initially improve the forecast when assessed on monitoring stations not used in assimilation. However, as the forecast length increased, the forecast converged towards the reference simulations where no data assimilation was used. The relaxation time was 6-12 hours for SO_2 and NO_2 and about 24 hours for O_3.

An alternative assimilation scheme was tested for SO_2. In addition to the initial state of the forecast, the scheme adjusted the gridded emission fluxes based on the observations within the last 24 hours. The improvements due to adjustment of emissions were generally small but, where observed, the improvements persisted throughout the 48 hour forecast.

The assimilation scheme was further adapted for estimating emission fluxes in volcanic eruptions. Assimilating retrievals of the Infrared Atmospheric Sounding Interferometer (IASI) instrument allowed reconstructing both the vertical and horizontal profile of SO_2 emissions during the 2010 eruption of Eyjafjallajökull in Iceland. As a novel feature, retrievals of plume height were assimilated in addition to the commonly used column density retrievals. The results for Eyjafjallajökull show that the plume height retrievals provide a useful additional constraint in conditions where the vertical distribution would otherwise remain ambiguous.

Finally, the thesis presents a rigorous description and evaluation of a numerical scheme for solving the advection equation. The scheme conserves tracer mass and non-negativity, and is therefore suitable for regional and global atmospheric chemistry models. The scheme is particularly adapted for handling discontinuous solutions; for smooth solutions, the scheme is nevertheless found to perform comparably to other state-of-art schemes used in atmospheric models.

Publishing unit
Atmospheric Composition Research

Classification (UDC)
502.3 519.63 517.956.47

Keywords
dispersion models, air quality, data assimilation, inverse modelling, numerical methods

ISSN and series title
0782-6117 Finnish Meteorological Institute Contributions

ISBN
978-952-336-011-2 (paperback)
978-952-336-012-9 (pdf)

Language
English

Pages
132

Acknowledgements

This thesis consists of research carried out during 2008–2016 in the Finnish Meteorological Institute. I thank my doctoral advisor, Dr. Mikhail Sofiev for introducing me to the atmospheric sciences and data assimilation, and I am grateful to my supervisors Dr. Ari Karppinen, Prof. Jaakko Kukkonen and Prof. Heikki Lihavainen at the Atmospheric Composition unit for their support. I also acknowledge the funding from Academy of Finland, the European Commission, European Space Agency and NordForsk which made this work possible.

I am honoured to have Dr. Adrian Simmons as my opponent. I thank my custos, Prof. Veli-Matti Kerminen for his support and guidance, and my pre-examiners Dr. Joakim Langner and Prof. Wouter Peters for their thorough and detailed reviews. I thank my coauthors for fruitful collaboration, and my colleagues at FMI for all the discussions.

Finally, I am grateful to my family for their continuing support. And to Marje, for everything.

Contents

List of publications

This thesis consists of an introductory review followed by 4 research articles. In the introductory review, the papers are cited according to their roman numerals.

I Vira, J., Sofiev, M., 2012. On variational data assimilation for estimating the model initial conditions and emission fluxes for short-term forecasting of SOx concentrations. *Atmos. Environ.* 46, 318–328. doi:10.1016/j.atmosenv.2011.09.066

II Vira, J., Sofiev, M., 2015. Assimilation of surface NO2 and O3 observations into the SILAM chemistry transport model. *Geosci. Model Dev.* 8, 191–203. doi:10.5194/gmd-8-191-2015

III Vira, J., Carboni, E., Grainger, R.G., Sofiev, M., 2016. Variational assimilation of IASI SO2 plume height and total-column retrievals in the 2010 eruption of Eyjafjallajökull using the SILAM v5.3 chemistry transport model. *Geosci. Model Dev. Discuss.* 1–28. doi:10.5194/gmd-2016-200

IV Sofiev, M., Vira, J., Kouznetsov, R., Prank, M., Soares, J., Genikhovich, E., 2015. Construction of the SILAM Eulerian atmospheric dispersion model based on the advection algorithm of M. Galperin. *Geosci. Model Dev.* 8, 3497–3522. doi:10.5194/gmd-8-3497-2015

Review of the papers and the author's contribution

Paper I discusses an assimilation experiment targeting the sulphur dioxide in central and southern Europe. The conventional assimilation approach where the prognostic variables (concentration in air) are updated was compared to a scheme where the emission forcing was refined in addition to the concentration in air. I wrote the assimilation code, designed and carried out the assimilation experiments and analysed the results. The paper was written in collaboration with Mikhail Sofiev.

Paper II presents a scheme for assimilating surface observations of ozone and nitrogen dioxide, and evaluates its performance in both forecast and reanalysis applications. I implemented the assimilation method, ran the simulations, analysed the results and wrote the paper.

Paper III extends the 4D-Var assimilation method into inverse modeling of volcanic emissions. As an application, the sulphur dioxide emissions in the 2010 eruption of Eyjafjallajökull were reconstructed using data from the IASI satellite instrument. I formulated and implemented the inversion method, ran the simulations, analysed the results and wrote the paper with the exception of section describing the satellite retrievals.

Paper IV evaluates an numerical advection scheme and describes its coupling to the SILAM chemistry transport model. I devised a modification to the original scheme, which significantly improved its performance for realistic flows. I also outlined its theoretical description (Section 2.2), performed the numerical tests discussed in Section 3.5 and contributed to the manuscript preparation.

1 Introduction

The success of numerical weather prediction, along with the increasing computing capability, has made numerical simulations feasible for diverse scientific and practical problems related to the atmospheric composition. Predicting dispersion of a hazardous pollutant, modelling regional air quality or simulating global distribution of aerosols and reactive gases are typical applications for the current chemistry transport models.

However, any prediction given by an atmospheric model is uncertain. In weather prediction, much of the uncertainty has been attributed to errors in the initial state (Magnusson and Källén, 2013). This is a consequence of the nonlinear dynamics (Lorenz, 1963, 1982) that govern the atmospheric flow, and thus, a skillful weather forecast needs to be initialised using current observations in the process known as data assimilation, defined by Talagrand (1997) as "the process through which all the available information is used in order to estimate as accurately as possible the state of the atmospheric or oceanic flow".

This definition describes the data assimilation from the perspective of numerical weather prediction. In that sense, the first applications of data assimilation in tropospheric chemistry and dispersion modelling date back to late 90s (Elbern et al., 1997). Meanwhile, observations have been used in numerous inverse modelling studies aiming at estimation of emissions from point sources (see, for example, the review of Shankar Rao (2007)) or for estimation of greenhouse gas fluxes (Enting and Mansbridge, 1989; Houweling et al., 1999; Enting, 2002). The concept of data assimilation in atmospheric chemistry models is thus somewhat ambiguous. This thesis covers both inverse modelling of emissions and data assimilation in the traditional sense and explores the connection between the two.

The diversity of approaches to chemical data assimilation reflects the diversity of forecast problems in atmospheric chemistry and pollutant dispersion. Modelling the composition of polluted boundary layers is characterised by strong emission forcing and dissipation due to removal processes, and often strong chemical coupling between species. Due to the strong forcing and limited chemical lifetime of pollutants, perturbations in the initial state tend to dissipate rather than grow in time. As demonstrated by this thesis and previous studies discussed in Section 3.2, this sets a fundamental limit on the forecast improvements obtainable with data assimilation taken in its narrow definition.

Contrary to air quality modelling, simulating the dispersion of accidental releases or volcanic plumes usually involves a single, poorly known emission source. The combined uncertainty and importance of the source term makes this type of problem attractive for inverse modelling of emissions. However, the atmospheric lifetime of volcanic plumes is often longer than the lifetime of pollutants emitted near surface, and traditional data assimilation has indeed been found to improve long-range predictions of volcanic plumes (Flemming and Inness, 2013).

Inverse modelling generally requires confidence on the quality of the numerical model, which can be achieved by the appropriate choice of numerical methods and their sufficient evaluation. This aspect is addressed by the final part of this thesis, which describes the development and evaluation of a numerical scheme for

the advection equation, which forms a fundamental component in any chemistry transport model.

In summary, the main objectives of this thesis are as follows:

- To assess the impact of chemical data assimilation on short-term forecasts of gas-phase pollutants
- To evaluate a variational data assimilation scheme based on short-term emission adjustments
- To formulate a variational method for reconstructing temporal and vertical profiles of volcanic emissions using satellite retrievals
- To assess the added value of assimilating plume height retrievals for estimating the vertical profiles of sulphur emissions in explosive volcanic eruptions
- To evaluate a numerical scheme for solving the advection equation using up-to-date benchmarks.

This thesis consists of an introduction and four manuscripts. Paper I and Paper II approach data assimilation and inverse problems from the perspective of air quality forecasting; Paper III discusses inverse modelling of volcanic emissions, and Paper IV is about numerical solution the advection equation.

The introduction, which summarises the findings presented in the manuscripts, is organised as follows. Section 2 presents the theoretical background regarding numerical methods for the advection equation. Section 3 gives a brief overview of inverse problems, their connection to data assimilation, and and presents a review of their recent applications in atmospheric chemistry and dispersion models. Sections 5 and 6 present the main results and conclusions of the thesis.

2 Numerical modelling of pollutant transport

Extensive efforts regarding numerical methods in atmospheric chemistry models have been devoted to treatment of the advection equation

$$\frac{\partial \varphi}{\partial t} + \nabla \cdot (\varphi \mathbf{v}) = 0, \tag{1}$$

where φ denotes the species concentration, or equivalently,

$$\frac{\partial \psi}{\partial t} + \nabla \psi \cdot \mathbf{v} = 0, \tag{2}$$

where ρ denotes air density and $\psi = \varphi/\rho$ is the mixing ratio.

Numerical solution of Eq. (1) is also the main topic of Paper IV, which describes development of the advection scheme used in the SILAM chemistry transport model. This section gives a short introduction to the numerical methods used to solve Eq. (1) in atmospheric chemistry models. The emphasis is on conservative semi-Lagrangian methods – more general reviews of advection schemes have been given by Rood (1987) and Lauritzen et al. (2014).

The advection equation (1) is a component in the system of equations solved by chemistry transport models – namely, the tracer continuity equation

$$\frac{\partial \varphi}{\partial t} + \nabla \cdot (\varphi \mathbf{v}) - \nabla \cdot \mathbf{K} \nabla \varphi = R(\varphi, x, t) \tag{3}$$

where $\mathbf{v}(x, y, z, t)$ is wind field, $\mathbf{K}$ is the eddy diffusivity tensor and R denotes the sources and sinks. For chemically reactive species, R includes reactions with other species, and in this case, (3) becomes a system of partial differential equations non-linearly coupled by the reaction term.

The equation (3) needs to be solved numerically. An almost universally used approach is the operator splitting, where the terms in Eq. (3) are solved in separate, sequential steps. This uncouples the transport equation of chemically connected constituents from each other, and enables using explicit or implicit time integration depending on the typical time scale of each term separately. The splitting can be extended to solving multidimensional operators sequentially in each dimension; this is called dimensional splitting. Operator splitting introduces additional numerical errors which have been discussed for the advection-reaction-diffusion system by Lanser (1999), Sportisse (2000) and Santillana et al. (2016).

Due to the requirement of strict mass conservation, numerical solution of (1) in atmospheric chemistry models (as reviewed by Kukkonen et al. (2012)) is most commonly based on the integral form of Eq. (1):

$$\frac{\mathrm{d}}{\mathrm{d}t} \int_{\Omega_i} \varphi(x) d\Omega = - \oint_{\partial \Omega_i} \varphi(x) \mathbf{v} \cdot \mathbf{n} dS, \tag{4}$$

which is readily obtained using the divergence theorem. Here, Ω_i denotes the ith grid cell and $\mathbf{n}$ is the unit normal vector.

If the flux integrals on the right hand side of Eq. (4) are approximated numerically, one obtains a spatially discrete system for the cell-averaged concentration $\bar{\varphi}_i$, which in one dimension can be written as

$$\frac{\mathrm{d}\bar{\varphi}_i}{\mathrm{d}t} = \frac{1}{h}(F_{i-1/2} - F_{i+1/2}), \tag{5}$$

where h is the cell size. The cross-boundary fluxes $F_{i\pm1/2}$ are evaluated by fitting a polynomial or other interpolant to the mean concentrations $\bar{\varphi}_i$ of the neighbouring grid cells.

Due to the Courant-Friedrichs-Lewy (CFL) stability condition, schemes in the form (5) are only stable for sufficiently small Courant numbers $C = v\Delta t/h$, which usually needs to be less than one. This is especially problematic in global models using a lon-lat grid, since convergence of the meridians results in high Courant numbers near the poles.

The desire to choose the timestep based on accuracy rather than stability considerations has led to the popularity of the semi-Lagrangian advection schemes. In the semi-Lagrangian schemes, the numerical domain of dependence for each receiving grid cell is not restricted to the adjacent cells, but is instead determined by trajectory integrations. However, the classical gridpoint-based semi-Lagrangian advection methods used in weather prediction models (Staniforth and Côte, 1991) are not conservative, and thus rarely used in chemistry models.

Conservative semi-Lagrangian schemes can be constructed based on the Lagrangian form of Eq. (4),

$$\frac{\mathrm{d}}{\mathrm{d}t}\int_{\mathcal{V}(t)} \varphi(x) d\Omega = 0, \tag{6}$$

where the Lagrangian volume $\mathcal{V}$ follows the flow. The discretisation of Eq. (6) can proceed in several ways, which will be discussed here in single space dimension. A detailed presentation of conservative semi-Lagrangian schemes in two or three dimensions has been given by Lauritzen et al. (2011).

Given the concentration $\varphi(x, t_{k-1})$ at previous timestep, the mean concentration in grid cell Ω_i at the next timestep can be evaluated by integrating over the departure cell $\Omega_i(t_{k-1})$, as shown in Fig. 1a,

$$\bar{\varphi}_i = \frac{1}{|\Omega_i(t_{k-1})|}\int_{\Omega_i(t_{k-1})} \varphi(x, t_k) d\Omega, \tag{7}$$

where $|\Omega_i(t_{k-1})|$ denotes the volume of the departure cell, which is determined by integrating the backward trajectories from the cell borders $x_{i\pm1/2}$. The continuous concentration $\varphi(x, t)$ is unknown and needs to be evaluated from an interpolation, $\widetilde{\varphi}(x)$, often called a reconstruction function, which has a similar role as the interpolation used in Eulerian schemes represented by Eq. (5). However, contrary to the flux-form schemes, the reconstruction function must be conservative:

$$\int_{\Omega_i} \widetilde{\varphi}(x) dx = |\Omega_i|\bar{\varphi}_i. \tag{8}$$

It would be equally possible to compute forward trajectories from Ω_i and integrate over intersections of the receiving Eulerian cells and the arrival volume (Fig.

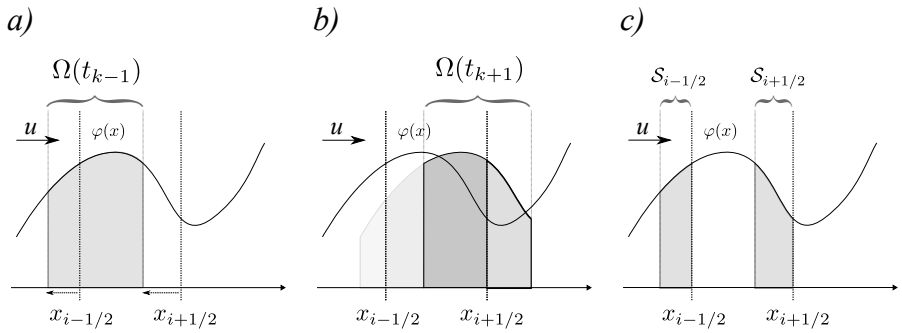

Figure 1: Semi-Lagrangian advection in one dimension: a) a backwards scheme with integration over departure cell; b) a forward scheme with distribution of mass between cells i and $i+1$; c) a flux scheme with integration over swept volumes $\mathcal{S}_{i-1/2}$ and $\mathcal{S}_{i+1/2}$.

1b). However, the backward integration allows the reconstruction functions $\widetilde{\varphi}(x)$ to be defined with respect to the fixed (Eulerian) grid, which is often simpler.

Alternatively, a flux-form scheme can be also constructed following the Lagrangian approach. This follows from the observation that the time integral of a flux through a cell interface can be represented as an integral over the volume which passes through the interface during the timestep:

$$\int_{t_k}^{t_{k+1}} F_{i-1/2}(t)dt = \int_{\mathcal{S}_{i-1/2}} \widetilde{\varphi}(x, t_k)dV. \tag{9}$$

The idea is illustrated in Fig. 1c. Since the "swept volume" $\mathcal{S}$ can span several grid cells, the scheme is not limited by the typical CFL condition. A flux-form scheme is conservative even if the reconstruction function does not satisfy Eq. (8), or if the integrals are approximated numerically.

Fully multidimensional, conservative semi-Lagrangian schemes have been described by Nair and Machenhauer (2002) and Lauritzen et al. (2010). Tracking the Lagrangian volumes $\Omega(t)$ in a multidimensional flow is considerably more complex than in the one-dimensional case. However, at least for simulations with complex chemistry, the computational cost per tracer can remain reasonable, since the departure volume needs to evaluated only once for each cell.

A more straightforward way to extend the semi-Lagrangian computations to multiple dimensions is to use dimensional splitting as done in the flux-form semi-Lagrangian scheme of Lin and Rood (1997), and in the scheme described Paper IV. Dimensional splitting is also used in many purely Eulerian schemes (Bott, 1989; Prather, 1986; Colella and Woodward, 1984).

In addition to mass conservation, desirable qualitative features for a numerical advection include positive definiteness (preservation of non-negativity) and monotonicity with regard to the initial data. As discussed by LeVeque (1992), a prac-

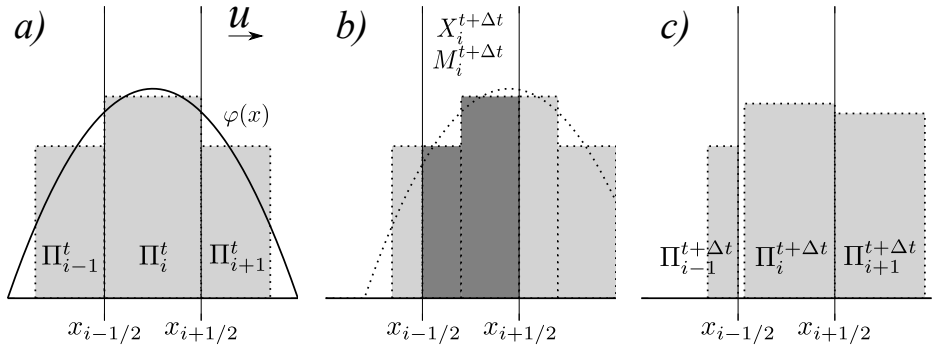

Figure 2: The advection scheme of Galperin (1999): a) the continuous function $\varphi(x)$ is represented by box functions Π; b) the box functions are transported with the flow and new centres of mass X_i and total masses M_i are evaluated; c) the box functions Π_i are updated according to the new X_i and M_i.

tically useful definition for the monotonicity is that for a monotonously increasing (or decreasing) initial condition, the numerical solution at a later time has to be monotonously increasing (decreasing). This property is sufficient to guarantee that the scheme does not produce spurious oscillations near an isolated discontinuity.

A classical result is the theorem of Godunov (1959), which states that a monotonicity preserving linear finite difference scheme can be at most first order accurate. It is straightforward to show that a positive definite linear scheme will unavoidably be also monotonicity preserving. Due to the excessive diffusiveness of first-order schemes, the advection schemes used in chemistry transport models almost invariably include some nonlinear elements.

The advection scheme of Galperin (1999), developed and evaluated further in Paper IV, is a forward semi-Lagrangian finite volume scheme corresponding to the case b) in Fig. 1. For each grid cell, the scheme tracks the total mass M_i and centre of mass X_i given by

$$M_i = \int_{\Omega_i} \varphi(x)dx \tag{10}$$

$$X_i = \frac{1}{M_i}\int_{\Omega_i} x\varphi(x)dx. \tag{11}$$

The reconstruction function is a rectangular pulse show in Fig. 2a:

$$\Pi_i^k(x) = \begin{cases} \frac{M_i}{2w}, |x - X_i| \leq w \\ 0, \text{otherwise} \end{cases}, \tag{12}$$

where $w = \min(|X_i - x_{i-1/2}|, |X_i - x_{i+1/2}|)$ and $x_{i\pm1/2}$ are the cell borders. The full continuous distribution is therefore represented by the sum of Π_i:

$$\bar{\varphi}(x) = \sum_i \Pi_i(x). \tag{13}$$

Both M_i and X_i are updated (Fig. 2 panels b and c) using $\Pi_i(x)$, whose form allows the necessary integrals to be evaluated exactly. Since $\Pi_i(x) \geq 0$ for all x and i, the scheme conserves non-negative solutions. However, as discussed in Paper IV, the scheme is otherwise not fully monotonicity preserving.

Use of additional prognostic quantities (X_i) connects the scheme to Eulerian schemes of Russell and Lerner (1981) and Prather (1986). The reconstruction function given by Eq. (12) distinguishes the scheme from the otherwise similar scheme of Egan and Mahoney (1972), which does not adjust the width w, but instead tracks the second moments. Also, the Egan and Mahoney (1972) scheme is formulated in Eulerian context and is only stable conditionally to the Courant number.

3 Inverse problems and data assimilation

Physical models normally predict values of an observable quantity given a set of known input parameters. In mathematical literature (Tarantola, 2005), this is often referred as the forward problem. Conversely, if the input parameters are poorly known and need to be evaluated from a set of observed values, an inverse problem needs to be solved. As it turns out, the concept of inverse problems connects quite naturally with the process called data assimilation in meteorology and related fields. This section aims to offer a unified view to the two concepts.

3.1 Theoretical background

The forward problem can be formalised as

$$\mathbf{y} = \mathcal{H}(\mathbf{x}), \tag{14}$$

where $\mathbf{x}$ and $\mathbf{y}$ are vectors denoting the input parameters and observations which are connected by the operator $\mathcal{H}$. In the following discussion, operators which may be nonlinear are denoted with calligraphic letters such as $\mathcal{H}$, while the boldface letters (eg. $\mathbf{H}$) denote matrices and linear operators.

Since the vectors $\mathbf{x}$ and $\mathbf{y}$ usually have different dimensions, inverting Eq. (14) does generally not constitute a well-posed problem. Moreover, in many problems related to atmospheric constituent transport, features of the forward operator $\mathcal{H}$ render techniques like ordinary least squares ill-conditioned, and to overcome this difficulty, the inverse problem needs to be modified in some sense. One approach is regularisation, where a well-posed "nearby" problem is solved with the hope of arriving at an approximate solution of the original problem. A very common example is the Tikhonov regularisation, which in the simplest form formulates the inversion as a penalised least-squares problem of minimising

$$\mathcal{J}(\mathbf{x}) = \|\mathbf{y} - \mathcal{H}(\mathbf{x})\|^2 + \alpha^2 \|\mathbf{x}\|^2, \tag{15}$$

where the parameter α^2 controls the level of regularisation.

Alternatively, the inversion can be viewed as a Bayesian estimation problem where the ill-posedness is addressed by including additional a priori information, formulated as the prior probability distribution $p(\mathbf{x})$. To quantify the uncertainty of observations, Eq. (14) is recast into a stochastic form

$$\mathbf{y} = \mathcal{H}(\mathbf{x}) + \epsilon, \tag{16}$$

where ϵ denotes the observation errors. The solution of the inverse problem is then formally the probability distribution of $\mathbf{x}$ conditioned to a realisation of $\mathbf{y}$, $p(\mathbf{x}|\mathbf{y})$, as given by the Bayes theorem

$$p(\mathbf{x}|\mathbf{y}) = \frac{p(\mathbf{x})p(\mathbf{y}|\mathbf{x})}{p(\mathbf{y})}. \tag{17}$$

In principle, the posterior distribution $p(\mathbf{x}|\mathbf{y})$ could be characterised in many ways, including moments or quantiles, but the computational cost of $\mathcal{H}$ often limits

the choice of estimators. An option which does not require a drawing a large sample from the posterior distribution is the maximum a posteriori (MAP) estimate of $\mathbf{x}$ given by

$$\mathbf{x}_{\mathrm{MAP}} = \arg\max_{\mathbf{x}} p(\mathbf{x}|\mathbf{y}). \tag{18}$$

The MAP estimate can be evaluated using numerical optimisation methods provided that the density function $p(\mathbf{x}|\mathbf{y})$ is known. For some probability distributions (most notably Gaussian), $\mathbf{x}_{\mathrm{MAP}}$ is also equal to the conditional mean $E(\mathbf{x}|\mathbf{y})$.

To connect the discussion of general inverse problems with data assimilation, we next assume that $\mathbf{x}$ in fact represents the state of a stochastic process given by

$$\mathbf{x}_{k+1} = \mathcal{M}_k(\mathbf{x}_k) + \delta_k, \tag{19}$$

where the model operator $\mathcal{M}$ propagates the state vector between the timesteps k and δ represents the model noise. The problem is now to estimate the state $\mathbf{x}$ using simultaneously the observations given by Eq. (16) and knowledge of the system evolution encoded into Eq. (19).

The form of Eq. (19) suggests towards a recursive scheme for estimating the distribution of $p(\mathbf{x}_k|\mathbf{y}_0...\mathbf{y}_k)$ conditioned to observations until step k. The recursion proceeds in two steps:

1. Analysis step: given the prior (or *background*) distribution $p(\mathbf{x}_k|\mathbf{y}_0...\mathbf{y}_{k-1})$ and the current observations $\mathbf{y}_k$, characterise the posterior (or *analysis*) distribution $p(\mathbf{x}_k|\mathbf{y}_{i\leq k})$.

2. Forecast step: given $p(\mathbf{x}_k|\mathbf{y}_{i\leq k})$ and Eq. (19), characterise the conditional distribution of the forecast $p(\mathbf{x}_{k+1}|\mathbf{y}_{i\leq k})$, which becomes the prior distribution for the next analysis step.

Linear observation and model operators $\mathcal{H}$ and $\mathcal{M}$ combined with a Gaussian initial distribution $p(\mathbf{x}_0)$ and noise terms δ and ϵ form an important special case where all the involved conditional distributions are also Gaussian. The Gaussian distributions are completely determined by their conditional means and covariances, which in turn can be evaluated algebraically. This procedure leads to the well-known Kalman filter, which at each analysis and forecast step updates both the conditional mean and covariance matrix of $\mathbf{x}_k$.

The requirement to manipulate the covariance matrices of the model state makes the standard Kalman filter suitable only for relatively low-dimensional systems. However, the Ensemble Kalman filter (EnKF, Evensen (1994, 2003)) has proven to be a feasible option even for large-scale geophysical models. Ignoring the covariance propagation and instead using a prescribed covariance matrix for the analysis step leads to another important class of assimilation methods which, in particular, includes the variational methods (Le Dimet and Talagrand, 1986; Lorenc, 1986) used in this work.

The variational methods usually assume that the observation errors are Gaussian and unbiased, and that the background distribution $\mathbf{x}_k|\mathbf{y}_{i<k}$ is also Gaussian:

$$\begin{aligned} \mathbf{x}_k|\mathbf{y}_{i<k} &\sim \mathcal{N}(\mathbf{x_b}, \mathbf{B}) \\ \epsilon &\sim \mathcal{N}(0, \mathbf{R}), \end{aligned} \tag{20}$$

Using the background state $\mathbf{x}_b$ and the background and observation error covariance matrices $\mathbf{B}$ and $\mathbf{R}$, the variational methods aim to evaluate a MAP estimate for the analysis state $\mathbf{x}_a$. The background error covariance matrix is usually not defined explicitly but instead as an operator acting on $\mathbf{x}$, which avoids the computational difficulties associated with its high dimension.

Under the assumptions (20), the posterior probability density is maximised by minimising the cost function

$$\begin{aligned} \mathcal{J}_{3D}(\mathbf{x}) &= \frac{1}{2}(\mathbf{y}-\mathcal{H}(\mathbf{x}))^T\mathbf{R}^{-1}(\mathbf{y}-\mathcal{H}(\mathbf{x})) \\ &+ \frac{1}{2}(\mathbf{x}-\mathbf{x_b})^T\mathbf{B}^{-1}(\mathbf{x}-\mathbf{x_b}). \end{aligned} \tag{21}$$

Minimising the cost function $\mathcal{J}(\mathbf{x})$ with an iterative, gradient-based method yields the data assimilation scheme known as the three-dimensional variational assimilation, or 3D-Var (Lorenc, 1986). The gradient of the cost function is given by

$$\nabla\mathcal{J}_{3D}(\mathbf{x}) = -\mathbf{H}^*\mathbf{R}^{-1}(\mathbf{y}-\mathcal{H}(\mathbf{x})) + \mathbf{B}^{-1}(\mathbf{x}-\mathbf{x}_b), \tag{22}$$

where the adjoint observation operator $\mathbf{H}^*$ is related to the linearised observation operator $\mathbf{H}$ by the duality relation

$$\langle \mathbf{H}\psi, \varphi\rangle = \langle \psi, \mathbf{H}^*\varphi\rangle \tag{23}$$

for any pair of vectors φ, ψ belonging to the observation and model space, respectively.

Algorithms which use observations to update the past in addition to the current model state are called smoothers. The most important data assimilation algorithm in this category is the four-dimensional variational assimilation (4D-Var) method. Normally, 4D-Var (Le Dimet and Talagrand, 1986) is used in the strong-constraint form which estimates the system state within an assimilation window, during which the model noise δ_k is assumed negligible. This implies that the evolution of $\mathbf{x}_k$ is determined by the state $\mathbf{x}_0$ in the beginning of the assimilation window. Under the assumptions of Eq. (20), this results in a cost function

$$\begin{aligned} \mathcal{J}_{4D}(\mathbf{x}_0) &= \frac{1}{2}\sum_{k=0}^{n}(\mathbf{y}_k-\mathcal{H}_k(\mathbf{x}_k))^T{\mathbf{R_k}}^{-1}(\mathbf{y_k}-\mathcal{H}_k(\mathbf{x}_k)) \\ &+ \frac{1}{2}(\mathbf{x}_0-\mathbf{x_b})^T\mathbf{B}^{-1}(\mathbf{x}_0-\mathbf{x_b}), \end{aligned} \tag{24}$$

with $x_{k+1} = \mathcal{M}_k(\mathbf{x}_k)$ for each $0 \le k < n$. By considering a first order perturbation, it is easy to show that the gradient of $\mathcal{J}_{4D}(x)$ with respect to the initial state is given by

$$\nabla\mathcal{J}_{4D}(\mathbf{x}_0) = -\sum_{k=0}^{n}\mathbf{M}^*_{k,0}\mathbf{H}^*_k\mathbf{R}_k^{-1}(\mathbf{y}_k-\mathcal{H}(\mathbf{x}_k)) + \mathbf{B}^{-1}(\mathbf{x}_0-\mathbf{x}_b), \tag{25}$$

where $\mathbf{M}^*_k$ is the adjoint model operator defined analogously to the adjoint observation operator $\mathbf{H}^*_k$ and $\mathbf{M}^*_{k,0}$ is shorthand for $\mathbf{M}^*_0\mathbf{M}^*_1...\mathbf{M}^*_k$. The first term in the

gradient is in practice obtained by backwards integration of the adjoint system

$$\mathbf{x}_k^* = \mathbf{M}_k^* \mathbf{x}_{k+1}^* - \mathbf{H}_k^* \mathbf{R}_k^{-1}(\mathbf{y}_k - \mathcal{H}_k(\mathbf{x})). \tag{26}$$

Compared to evaluating a 3D-Var analysis separately for each time within the assimilation window, the 4D-Var method uses the prescribed background error covariance matrix $\mathbf{B}$ only in the beginning of the window. Within the assimilation window, the forward and adjoint model integrations in 4D-Var result in implicit propagation of the background errors to the later timesteps, which generally makes the 4D-Var analysis more accurate than 3D-Var even in the end of assimilation window.

Another useful consequence of the implied covariance evolution is that 4D-Var can dynamically estimate unobserved components in the state vector, which finally returns us to the inverse problem of estimating an emission forcing given a set of tracer measurements.

In a chemistry model, the state vector $\mathbf{x}_k$ consists of tracer concentrations. The emission fluxes are introduced as a forcing $\mathbf{f}$,

$$\mathbf{x}_{k+1} = \mathcal{M}_k(\mathbf{x}_k) + \mathbf{f}_{k+1}, \tag{27}$$

where each $\mathbf{f}_k \sim \mathcal{N}(\mathbf{f}_k^b, \mathbf{K}_k)$ is Gaussian and to be estimated along with $\mathbf{x}_0$. The 4D-Var cost function for this system is

$$\begin{aligned} \mathcal{J}_f(\mathbf{x}_0, \mathbf{f}_1, ..., \mathbf{f}_n) &= \frac{1}{2}\sum_{k=0}^{n}(\mathbf{y}_k - \mathcal{H}_k(\mathbf{x}_k))^T {\mathbf{R}_\mathbf{k}}^{-1}(\mathbf{y}_\mathbf{k} - \mathcal{H}_k(\mathbf{x}_k)) \\ &+ \frac{1}{2}\sum_{k=0}^{n}(\mathbf{f}_k - \mathbf{f}_k^b)^T \mathbf{K}_k^{-1}(\mathbf{f}_k - \mathbf{f}_k^b) \\ &+ \frac{1}{2}(\mathbf{x}_0 - \mathbf{x}_\mathbf{b})^T \mathbf{B}^{-1}(\mathbf{x}_0 - \mathbf{x}_b). \end{aligned} \tag{28}$$

With a similar derivation as for Eq. (24), it can be shown that the gradient for $\mathcal{J}_f$ with respect to $\mathbf{f}_k$ is simply given by the adjoint variables $\mathbf{x}^*$ as

$$\frac{\partial \mathcal{J}_f(\mathbf{x}_0, \mathbf{f}_1, ..., \mathbf{f}_n)}{\partial \mathbf{f}_k} = \mathbf{x}_k^* + \mathbf{K}_i^{-1}(\mathbf{f}_k - \mathbf{f}_k^b) \tag{29}$$

The variational formulation of the flux inversion was presented by Elbern et al. (2000). However, Eq. (27) has the same form as the generic evolution equation (19). If the stochastic forcing $\mathbf{f}_k$ is interpreted as the model error, as in Eq. (19), then the problem (27) and its solution are similar to the technique of Derber (1989), later referred by Trémolet (2006) as a weak-constraint 4D-Var algorithm.

The most important complexity in implementing the 4D-Var method with an existing model lies within developing, testing and maintaining the code corresponding to the adjoint model and observation operators $\mathbf{M}^*$ and $\mathbf{H}^*$. This can be achieved with either manual or automatic transformation of the program code (Giering and Kaminski, 1998). The resulting code is referred as the discrete adjoint. The alternative approach is to start from the continuous system of equations, such as Eq.

(3), and derive the continuous adjoint system, typically also a partial differential equation. The adjoint system for the flux-form advection equation (1) is an equation similar to its advective form (2) (Marchuk, 1995; Elbern and Schmidt, 1999), which admits a similar numerical solution as the forward equation. Consequently, the continuous adjoint has been adopted for the advection component in several chemistry transport models (Henze et al., 2007; Hakami et al., 2007; Davoine and Bocquet, 2007), and the approach has proven successful even though the gradient obtained this way is only an approximation to Eq. (25). Furthermore, in the numerical tests of Gou and Sandu (2011), the continuous adjoints for advection were found preferable at least in an idealised setting; this was attributed to the nonlinearities in advection schemes mentioned in Section 2.

3.2 Applications in atmospheric chemistry and dispersion modelling

The preceding section showed that inverse modelling of the emission fluxes and chemical data assimilation can be handled by a similar formalism. However, on practical level, the past research has followed several largely distinct lines. The lines of research with influence on this thesis include (i) inverse studies of point sources, (ii) reactive gas flux inversions and (iii) studies on chemical data assimilation for air quality forecasting.

The first experiments with data assimilation in atmospheric chemistry models were with stratospheric chemistry models (Fisher and Lary, 1995) and some years later with tropospheric chemistry and aerosol models (Elbern and Schmidt, 1999; van Loon et al., 2000; Collins et al., 2001). Studies assessing the improvements of short term forecasts in addition to evaluating the analysis fields have been described by Elbern and Schmidt (2001), Blond and Vautard (2004) and Wu et al. (2008) for ozone and by Tombette et al. (2009) and Pagowski et al. (2010) for particulate matter.

For ozone and particulate matter, initialising the forecast from the analysis has been found to improve the forecast mainly within a range of 24 hours with a minor improvement for hours 24–48. Fewer studies have considered the impact of data assimilation on forecasts of nitrogen dioxide (NO_2) or other short-lived pollutants. Due to the shorter chemical lifetime, the forecast improvements can be expected to be transient, which was indeed confirmed by Wang et al. (2011), Silver et al. (2013), and Paper II.

In addition to the mainly regional model studies cited above, chemical data assimilation has been incorporated to global models. Due to the uneven coverage of the surface-based observation networks, the main attention in global applications has been on assimilating satellite retrievals of both aerosol (Benedetti et al., 2009; Zhang et al., 2008; Weaver et al., 2007) and gas-phase (Inness et al., 2013) constituents.

Inverse methods for source term estimation were first focused on accidental or intentional releases of radioactive tracers. The 4D-Var method was proposed by Robertson and Persson (1993) for estimating the intensity of a release with a known location and timing. Adjoint methods were later investigated also for locating the

source by Pudykiewicz (1998) and Issartel and Baverel (2003) and, as part of a more strictly Bayesian algorithm, by Bocquet (2007).

In the meantime, algorithms for estimating distributed (as opposed to point) sources were introduced for estimating emission fluxes of greenhouse gases (Kaminski et al., 1999; Peters et al., 2010; Peylin et al., 2013) and short-lived trace gases (Müller and Stavrakou, 2005; Miyazaki et al., 2012) in global scale. Especially in the early studies, the emissions were aggregated into a few (< 100) geographical regions, while the later studies have provided also fully gridded emission estimates.

Updating the emission fluxes as means to improve regional-scale air quality forecasts was investigated by Elbern et al. (2007). In a two-week experiment, adjusting the emission fluxes was found to result in additional and more persistent forecast improvement when compared to adjusting the initial condition only. On the other hand, Curier et al. (2012) assimilated ozone data to adjust fluxes of precursor species, and found the emission adjustments to have little temporal continuity, and consequently were unable to obtain significant forecast improvements by using the adjusted emissions. Paper I considers the approach of Elbern et al. (2007) with a focus on emissions of sulphur dioxide.

Inverse modelling of volcanic emissions usually has to rely on satellite retrievals of aerosols or trace gases. While the geographical location can be assumed known, the emitted amount and vertical distribution are uncertain. Inverse modelling using satellite data has been shown to be useful for estimating the vertical (Eckhardt et al., 2008), temporal (Boichu et al., 2013) or both vertical and temporal (Stohl et al., 2011) emission profiles in explosive volcanic eruptions. The low dimension of the parameter vector (emission as function of time and/or altitude) makes it possible to avoid the adjoint formalism (Eq. 29) and evaluate the required source-receptor matrix elementwise. The aforementioned studies are, nevertheless, based on quadratic cost functions similar to 4D-Var (Eq. 28). Alternative approaches focusing mainly on the vertical distribution have been presented in papers of Flemming and Inness (2013), Zidikheri and Potts (2015) and Heng et al. (2016).

The satellite retrievals previously used in inverse modelling of volcanic emissions have been for the column density (vertical integral) of volcanic ash or sulphur dioxide. Estimation of the vertical profile then depends on resolving the variation of transport patterns with regard to the injection height. This approach has been used successfully for several eruptions (Kristiansen et al., 2010; Moxnes et al., 2014); however, in absence of sufficient vertical wind shear, the inversion relies on a priori profile. In contrast, Paper III derives an observation operator for satellite-retrieved plume height. Using retrievals by the Infrared Atmospheric Sounding Interferometer (IASI), the study demonstrates that complementing the column density retrievals with the retrieved plume heights results in a more realistic vertical emission profile.

4 Model setup and input data

The studies which constitute this thesis use the SILAM chemistry transport model. This section gives a brief overview of the model and the input data used, while detailed descriptions of the model configurations and datasets are given in each publication. The input data described below apply to papers I, II and III. Paper IV is based on two-dimensional synthetic test cases with the main focus on the test suite proposed by Lauritzen et al. (2012).

4.1 The SILAM model

The SILAM (System for integrated modeling of atmospheric composition) model was initially developed as a Lagrangian particle model for emergency applications (Sofiev et al., 2006) and later evolved into an Eulerian chemistry-transport model (Sofiev et al. (2008) and Paper IV). In addition to the horizontal transport described in Paper IV, the model includes the vertical discretisation of Sofiev (2002) and the particle dry deposition scheme of Kouznetsov and Sofiev (2012). Dry deposition of gases as well as wet deposition of gases and particles is described by Sofiev et al. (2006).

The model is normally set up with a regular lon-lat grid. Except for the advection benchmarks in Paper IV, the studies in in this thesis use a limited area configuration with resolutions between 0.25° and 0.5°. The vertical grid is flexible; Paper I and Paper II use terrain-following z-levels reaching up to 7-9 km with vertical resolution decreasing from 30-40 meters in lowest layers to 2-3 km in the free troposphere. In Paper III, the maximum layer thickness is limited to 500 meters to better resolve the volcanic plumes injected into upper troposphere.

SILAM includes two chemistry mechanisms: the DMAT scheme of Sofiev (2000) describes formation of inorganic secondary aerosols and partitioning of nitrogen oxides, while all other photochemical processes, including ozone formation, are simulated with the Carbon Bond mechanism (CB4, Gery et al. (1989)). The CB4 mechenism is implemented using a three-stage Rosebrock solver generated by the Kinetic Pre-Processor software (Sandu and Sander, 2006). The DMAT mechanism is implemented manually following the quasi-steady-state approach.

The SILAM variational data assimilation system is described by the papers I, II and III in this thesis. The adjoint code used in papers I and III uses a continuous adjoint for advective transport and a manually developed adjoint for the DMAT sulphur chemistry; the diffusion and deposition processes are self-adjoint. The background error covariance operators are based on separation of dimensions as descibed by Singh et al. (2011). The quasi-Newton minimisation code of Gilbert and Lemaréchal (1989) is used with 3D-Var, while the bound-constrained L-BFGS-B code of Byrd et al. (1995) is used for emission inversions.

4.2 Emissions, boundary conditions and meteorology

The meterological fields used in this study originate to the ECMWF IFS weather prediction system; in Paper I and Paper II, operational forecasts are used while

Paper III uses the ERA-Interim reanalysis (Dee et al., 2011).

For anthropogenic emissions, Paper I uses the EMEP inventory valid for the year 2000. In Paper II, the TNO-MACC-II emission inventory (Kuenen et al., 2014) is used. In addition, the biogenic emissions of isoprene as simulated in Paper II using the model of Poupkou et al. (2010).

Paper II uses lateral boundary conditions from the MACC reanalysis (Inness et al., 2013). Paper I, which simulates only oxides of sulphur, does not use lateral boundary conditions; however, this is unlikely to affect the concentrations in the Central European subdomain, where the observations were assimilated.

4.3 Observational data

In Paper I and Paper II, hourly in-situ data of SO_2, NO_2 and ozone are assimilated. The data are extracted from the AirBase database compiled by the European Environment Agency. In Paper II, only the data from rural (for NO_2) or rural and suburban (for O_3) stations are used. In Paper I, data from all station types are assimilated. In both studies, part of the stations are witheld from assimilation and used for verifying the analysis fields.

Paper III uses satellite retrievals of Carboni et al. (2012) based on the observations of the Infrared Atmospheric Sounding Interferometer (IASI). The IASI instrument (Clerbaux et al., 2009) onboard the MetOp-A (since 2013, also MetOp-B) satellite is a Fourier transform spectrometer with a spectral range from 3.62 to 15.5 μm and a field of view of about 12 km at nadir. The dataset consists of retrievals of both column density and plume height of sulphur dioxide. For both parameters, the retrievals include rigorously derived error estimates which in turn are included in the inversion.

5 Results and discussion

5.1 Assimilation of air quality monitoring data

Paper I and Paper II study assimilation of in-situ trace gas observations into regional-scale simulations. In Paper I, a specific goal was to assess the usefulness of the gridded emission flux as a control variable in 4D-Var data assimilation. The goal of Paper II was to develop an analysis system with computational performance sufficient for long-term air quality reanalyses as well as operational, near-real time use. While the assimilation method is simpler, attention is given for estimating the statistical parameters affecting its performance.

In the study presented in Paper I, hourly SO_2 data at central European stations were assimilated in a two-week experiment, and effectiveness of the assimilation was evaluated in up to 48 h forecasts at stations not used in assimilation. Two approaches to assimilation were compared: the regular adjustment of forecast initial state using the 3D-Var method, and as an alternative, a 4D-Var assimilation scheme which estimates local variations in emissions of SO_2 in addition to the airborne concentrations. The refined emission fluxes were used to drive the subsequent forecast.

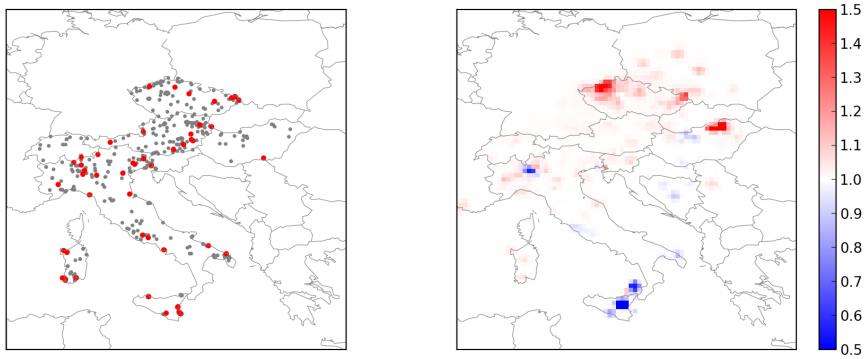

Figure 3: Assimilation experiment of Paper I. Left: location of the assimilation (grey) and control (red) stations. Right: emission correction factor after assimilation, average over two weeks.

The relative adjustments (a posteriori divided by a priori) to the SO_2 emissions, averaged over the two weeks, are shown in Fig. 3. In most areas, the average change is less than 5%. The strongest positive adjustments are obtained for limited areas in Hungary and Czech republic, while the most prominent reduction is obtained for the degassing emissions of volcano Etna.

The forecast impacts of assimilation were evaluated in terms of root mean squared error (RMSE). As seen from Fig. 4, the overall forecast improvements due to assimilation were mostly minor. The effect of 3D-Var diminished within 12

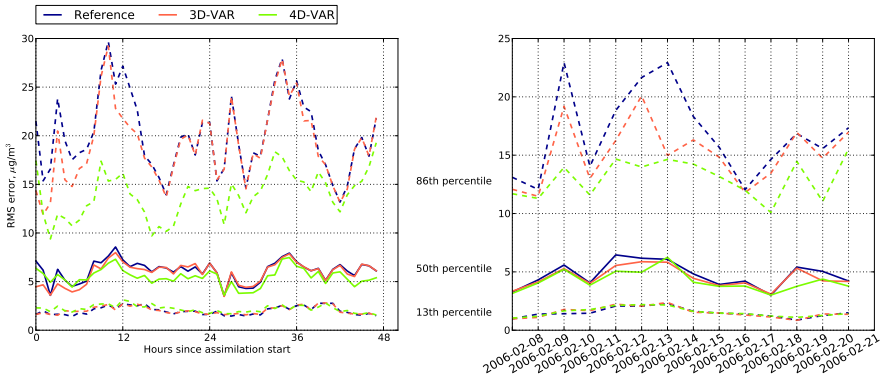

Figure 4: RMSE (μg m^{-3} for SO_2 on control stations as a function of forecast length (left) and in daily averages over assimilation windows (right). Figure 7 of Paper I.

hours of forecast, while with 4D-Var, a small but noticeable improvement persisted over the 48 hours. However, for a number of stations corresponding to the upper (86th) percentile of RMSE, the reduction was up to 50%.

The upper percentile turned out to include several stations near Etna, where the a priori simulations showed high SO_2 levels, and where the a posteriori emissions indicated systematic reductions throughout the two-week period. A feasible explanation to the reduction is that the degassing emissions, which were given on yearly level in the emission inventory, were not representative of the simulated period.

Paper II focuses on the prominent photochemical pollutants: hourly monitoring data of nitrogen dioxide (NO_2) and ozone (O_3) were assimilated in a European scale domain. The 3D-Var method was chosen mainly due to computational reasons; the system is aimed for reanalysis production in yearly and longer timescales. Special attention was given for estimating the observation and background error statistics, which in Paper I were based on ad-hoc values. The error statistics were calibrated with monthly simulations covering June and December 2011, and the obtained setup was subsequently tested in an assimilation experiment covering the year 2012.

The diagnostic identities presented by Desroziers et al. (2005) were used for estimating the observation error standard deviation σ_{obs} and the background error standard deviation σ_b, which together control the weighting between the model and observed values in the assimilation. Recently, Ménard (2016) analysed convergence the Desroziers method, and while he showed that estimating the full observation and background error covariance matrices is not possible, estimates of variance parameters, as done in Paper II, were found to converge provided that the assumptions of the parametrisation were satisfied.

The analysis errors were evaluated on stations excluded from assimilation. As a result of the improved diurnal and seasonal profiles for observation and background error standard deviations, the correlation coefficient and RMSE were improved

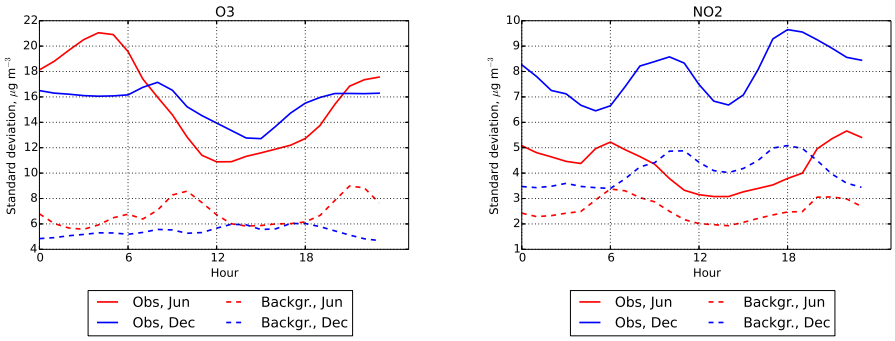

Figure 5: Diagnosed background (dashed) and observation error (solid lines) standard deviations (μgm^{-3}) on rural stations for O_3 (left) and NO_2 (right). Red lines correspond to the calibration made for June 2011, blue lines correspond to calibration for December 2011. Figure 4 in Paper II.

noticeably for both O_3 and NO_2. While the standard deviations were adjusted based on two months (June and December) in 2011, the improvement was valid throughout the simulated year 2012.

The obtained observation and background error standard deviations are shown in Fig. 5. The profiles are strikingly different from the first guess standard deviations, which were constant values 11.2 (σ_{obs}) and 20.6 (σ_b) μg m^{-3} for O_3 and 4.0 (σ_{obs}) and 8.0 (σ_b) μg m^{-3} for NO_2. Contrary to the first guess values, the estimated observation errors are larger than the corresponding background errors, which implies that the influence of an individual observation was reduced in comparison to the background field. The estimated observation and background errors also have a clear diurnal variation. For ozone, the variation is different for observation and background errors.

In addition to evaluating the effect of improved statistical parameters, the forecast impact of O_3 and NO_2 assimilation was evaluated over a three-week period which covered an ozone episode. The results (Fig. 6) demonstrate that for ozone, the effect of initialising the forecast from analysis diminishes within the first 24 forecast hours; the forecast of NO_2 relaxes to the background within 6-12 hours. The results regarding the short-lasting forecast improvement due to improved initial conditions are consistent the findings of previous studies: the forecast improvements for NO_2 have been limited to the range of a few hours in summer conditions (Wang et al., 2011; Silver et al., 2013); for ozone, improvements have been reported to extend from 24 to 48 h (Curier et al., 2012; Elbern et al., 2007).

Fewer studies have addressed SO_2. However, Elbern et al. (2007) found that the model bias was reduced for $\sim$ 24 forecast hours due to improved initial conditions. When also emission fluxes were adjusted similarly to Paper I, the forecast bias and RMSE were substantially reduced throughout the 48 hour forecast window. In the present work, neither of these results could be fully reproduced. The two studies are not immediately comparable due to differences in models, simulation domains

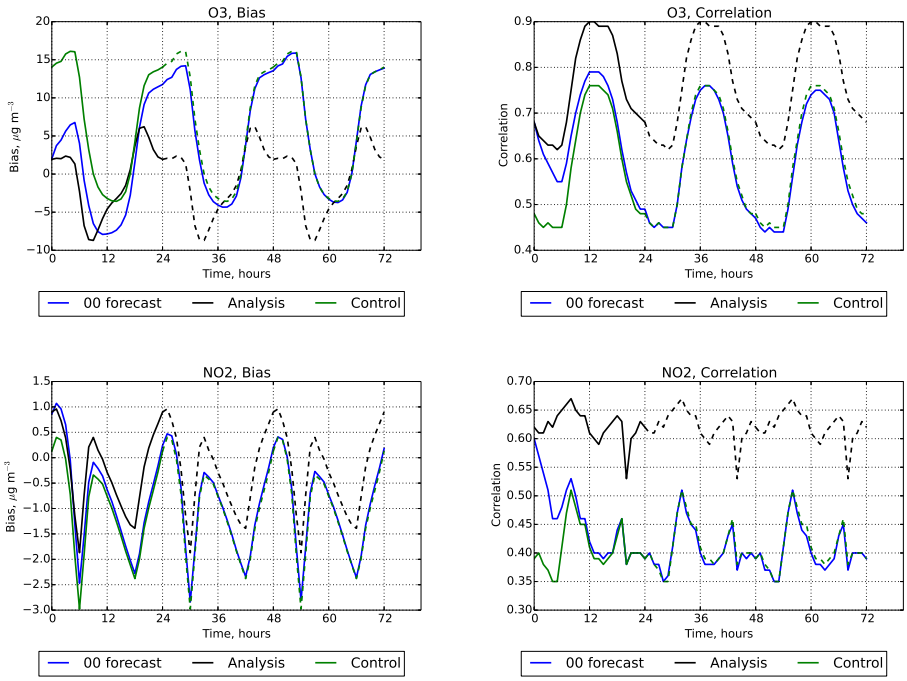

Figure 6: The model bias (μgm^{-3}) and correlation for O_3 (top) and NO_2 (bottom) at validation stations as a function of forecast length (blue lines). The corresponding indicators, the analyses (black) and control run (green), are shown averaged by time of day and replicated over the forecast window. Figures 7 and 8 in Paper II.

and the observational networks used. However, in the study of Elbern et al. (2007), the free-running model had a positive bias, which resulted in systematic reduction of a posteriori SO_2 emissions. In contrast, the emission adjustments in Paper I showed fewer systematic features. This could explain the different conclusions of the two studies, since using the adjusted emissions in forecasts is based on their assumed persistence.

The observation error estimates obtained in Paper II for NO_2 and ozone are somewhat higher than assumed in most previous studies. However, the errors for O_3 have similar magnitude as those estimated by Gaubert et al. (2014) using the same diagnostic relations but with the EnKF assimilation system and the CHIMERE chemistry transport model. The magnitude and diurnal variation of the observation errors is hardly explained by instrumental errors, but might be explained by representativeness errors, which arise from the discrepancy between the spatial scales represented by the model and the in-situ observations. The representativeness errors could be assumed to increase during night due to weaker mixing in the boundary layer, which would explain the strong summertime diurnal variation of σ_{obs} for O_3.

So far, the representativeness of in-situ data has been addressed mainly as a question of characterising the measurement stations (Henne et al., 2010; Joly and Peuch, 2012) and restricting the assimilation to the stations considered representative. Few studies have tried to explicitly quantify the representativeness errors in relation to the model resolution; however, Schutgens et al. (2016) estimated the magnitude of representativeness errors for satellite observations by aggregating data simulated at 10 km resolution, and found RMS differences reaching 30-160% between the high-resolution ("observation") and aggregated ("model") values. For air quality monitoring data, the relevant spatial and temporal scales might be smaller and more difficult to reach by modelling. However, representativeness errors can be included explicitly in the analysis scheme as shown by Koohkan and Bocquet (2012), which might provide a practical approach for assimilation studies.

5.2 Volcanic source term inversion using satellite data

Paper III builds on the work on variational assimilation presented in Paper I. However, the study was focused on estimating emission parameters (source term inversion) for the sulphur dioxide released in an individual eruption (Eyjafjallajökull in 2010). The location of eruption is assumed known, but the temporal and vertical variation are to be estimated. Instead of adjusting the emission source in steps of 24 hours, the inversion was performed in a single assimilation window covering 20 days.

The assimilated dataset consisted of satellite SO_2 retrievals of Carboni et al. (2012) from the Infrared Atmospheric Sounding Interferometer (IASI) instrument. The retrievals include both the column burden and plume height for SO_2, and an observation operator for joint assimilation of both quantities was developed in this work. The observation operator depends only on the vertical centre of mass and column density and thus sets only a partial constrain on the vertical profile. However, this approach avoids making additional assumptions on the shape or

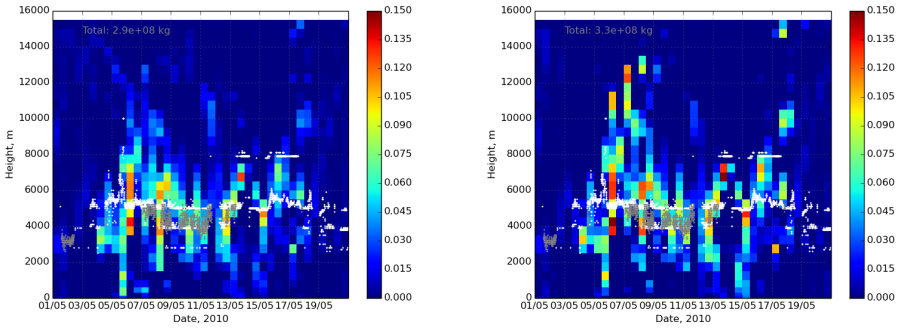

Figure 7: Emission flux (kg $m^{-1}s^{-1}$) of SO_2 in the Eyjafjallajökull eruption. Left: inversion using column density and plume height retrievals. Right: inversion using only column density retrievals. Figure 7 in Paper III.

thickness of the plume.

In Paper I, the background errors for the emission flux were defined subjectively. In an emission inversion, the assumed background error variance is equivalent to a regularisation parameter, which aims to balance the solution between the bias introduced by the a priori data and the noise introduced by the model and observation errors. Since the regularisation parameter is difficult to determine a priori, a nonparametric method referred as the L-curve (Hansen, 1992) was used in Paper III to estimate the regularisation parameter as a part of the inversion.

In the L-curve method, the inversion needs to repeated with different values of the regularisation parameter, which would be computationally expensive. However, as discussed by Fleming (1990) and Santos (1996), the iterative minimisation schemes used in 4D-Var yield by construction a sequence of solutions with decreasing regularisation. This feature of 4D-Var is rarely exploited in data assimilation, but the synthetic experiments in Paper III demonstrate that the regularised solutions obtained by truncating the 4D-Var iteration are practically equivalent to those obtained with the common Tikhonov regularisation.

The inversion results are shown in Fig. 7 which presents the emission rate of SO_2 as function of time and height. The plume height time series of Arason et al. (2011) are plotted together with the emission. The distribution of emissions obtained with and without plume height assimilation are largely similar. However, individual peaks reaching 12-15 kilometres height are strongly suppressed when the plume height retrievals are assimilated, which is consistent with the plume height time series.

The inversion gave an estimate of 0.29 Tg SO_2 emitted during the eruption. If only column load was assimilated, the emission increased to 0.33 Tg. The temporal and vertical profiles, integrated over the whole eruption, are shown in Fig. 8. The vertical distribution for SO_2 is quite similar to the vertical distribution obtained for volcanic ash by Stohl et al. (2011) despite the differences in the temporal distribution of the ash and SO_2 emissions.

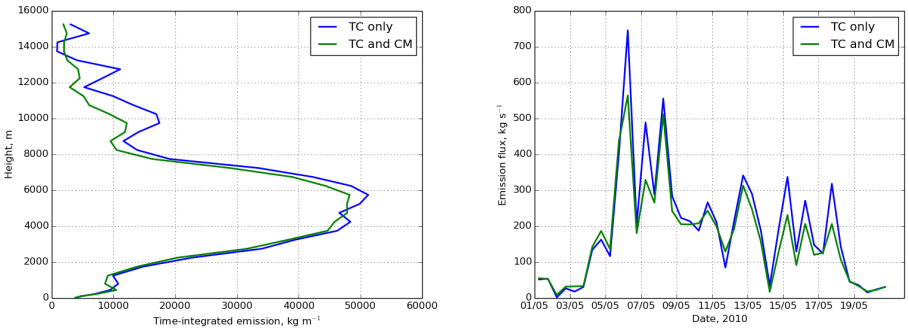

Figure 8: Emission of SO_2 in the Eyjafjallajökull eruption. Left: time-integrated vertical emission profile (kg m^{-1}); right: vertically integrated temporal profile (kg s^{-1}). Results with assimilation of both column density and plume height are shown in green, results with assimilation of column density only are shown in blue. Figures 8 and 9 in Paper III.

The 4D-Var method has previously not been applied in volcanic source term inversions. The 4D-Var inversion is equivalent to the linear algebraic method of Eckhardt et al. (2008), Stohl et al. (2011) and Boichu et al. (2013), which does not require adjoint model integrations. The main advantage of 4D-Var is in lower computational cost, although the difference is less important in short eruptions where the estimated emission has fewer degrees of freedom. Nevertheless, the observation operator for plume height developed in Paper III is applicable regardless of the inversion method, and the operator is also suitable for the traditional data assimilation which does not consider emission sources.

The variational method, as well as its algebraic counterpart, are based on assumption of a deterministic forward model, which makes realistic treatment of model errors difficult. The experiments with synthetic data presented in Paper III show that under fairly realistic assumptions, the model uncertainty has larger impact on the results than the observational noise. When real data are used, ad hoc modifications are frequently needed to obtain realistic inversion results. In Paper III, the retrieval errors were augmented with a constant model error term, while Boichu et al. (2013) kept only 10% of the zero-valued observations to improve the fit to data. However, more rigorous treatment of model uncertainty is difficult in the current inversion approach based on additive Gaussian errors.

During the 2010 Eyjafjallajökull eruption, a major limitation to the ash dispersion forecasts was the unpredictability of the emission source. Contrary to the continuous emissions studied in Paper I, the emissions in explosive eruptions have little persistence, and adjusting the emission fluxes is therefore unlikely to have inherent advantages when compared to adjusting the prognostic variable (airborne concentration). Although inverse modelling has been found to capture the vertical distribution of plumes better than a 4D-Var analysis (Kristiansen et al., 2017), ensemble or hybrid assimilation methods would allow more flexible treatment of the

transport model uncertainty.

5.3 Numerical solution of the advection equation

Paper IV evaluates a numerical scheme originally devised by (Galperin, 1999, 2000) for solving the advection equation, and discusses its incorporation to the SILAM. In its original form, the advection scheme produced strong artifacts especially in deformational flows associated with orographic uplifting. Paper I introduces a modification which substantially reduces magnitude of the artifacts. This version of scheme was implemented in the SILAM model and evaluated using a set of synthetic tests which aim to measure the scheme's performance for both smooth and discontinuous solutions.

As outlined in Section 2, in the Galperin's advection scheme, the solution is represented by discontinuous, rectangular pulses $\Pi(x)$, which at the beginning of timestep are confined to each grid cell. The scheme uses dimensional splitting, and the slabs are tracked along the one-dimensional flow $u(x)$. In the original version, the slabs were transported rigidly as

$$\Pi_i(x, t + \Delta t) = \Pi_i(x - u_i \Delta t, t), \tag{30}$$

where u_i is the velocity in the middle of cell i. This implies two problems: first, Eq. (30) is inaccurate if $u(x)$ changes quickly; second, if $u(x)$ changes sign within cell i, then $\Pi_i(x, t)$ remains almost unchanged. Together, these effects result in spurious accumulation of mass in areas where the atmospheric flow changes suddenly.

The improved version tracks separately the borders of Π_i, which allows the slab to deform with the flow and avoids the accumulations. The time integration for tracking Π_i was first changed to the second order implicit midpoint method, and in the finally published version, to the analytical solution for piecewise linear $u(x)$.

The two-dimensional tests introduced by Lauritzen et al. (2012) were used with various initial data to numerically evaluate the convergence and accuracy of the scheme. For a sufficiently smooth (Gaussian) initial condition, the rate of converge was near second order, and the absolute level of errors was lower when the scheme was run at a higher Courant numbers. Intuitively, the numerical errors in the Galperin scheme are due to the errors both in trajectory integration and in the Eulerian reconstruction (see Section 2). While the trajectory errors increase with increasing Courant number, the reconstruction errors are likely to decrease due to the fewer reconstructions needed, and thus, the optimal performance is achieved at some intermediate Courant number.

In the intercomparison study of Petrova et al. (2008), the Galperin scheme was found to spuriously steepen gradients in initially smooth solutions. This effect was confirmed in Paper IV, however, the presence of such steepening was found to depend nonlinearly on the initial condition. The nonlinearity, dissipation, and effective resolution of the scheme were studied further with spectral analysis.

In a one-dimensional periodic domain with 100 grid points, the scheme was run with sinusoidal initial conditions up to the 25th wavenumber. For each initial condition, the integration was repeated for a range of Courant numbers between 0 and 1. The scheme is then characterised by the amplification factor (ratio of

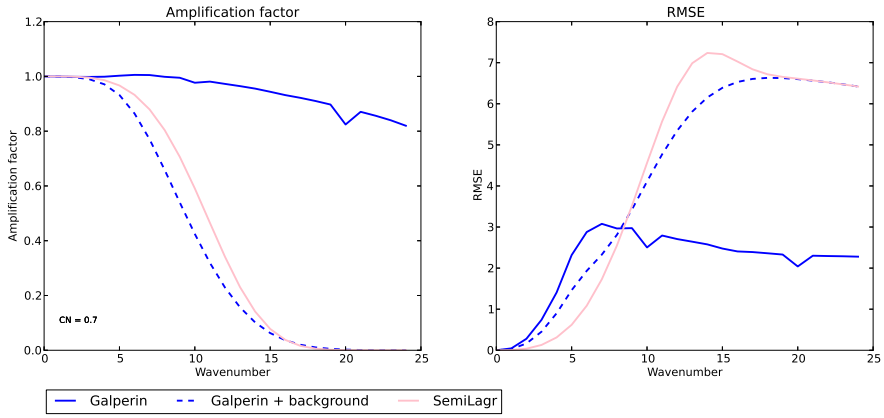

Figure 9: Amplification factor (left) and spectral RMSE (right) for 1D advection in a periodic domain. The Galperin scheme is shown for constant term 1.0 (solid blue) and 10.0 (dashed blue line). The results for a generic semi-Lagrangian scheme is in pink.

amplitudes of the initial and final solution) and root mean squared error (RMSE). Intuitively, the amplification factor measures the numerical diffusion which causes a scheme to loose details at smaller spatial scales. The spectrally resolved RMSE complements the amplification factor by including also the impact of phase errors and possible spurious modes.

Fig. 9 shows the amplification factor and spectral RMSE at the Courant number 0.7 as a function of the wavenumber up to $k = 25$. The results for Galperin scheme are shown for two cases: with no constant background (initial range from 0 to 1) and with a large constant background (initial range from 10 to 11). For comparison, the results for a generic, non-conservative semi-Lagrangian scheme with cubic interpolation are shown.

When the Galperin scheme is run without a background term, the amplification factor remains above 0.8 for all wavenumbers. The RMSE increases initially for k up to ~ 5, but shows otherwise little connection to the amplification factor, contrary to typical numerical schemes such as the cubic semi-Lagrangian scheme included in comparison. In presence of a background, the behaviour changes radically: all amplification factors are below or equal to one, and frequencies above $k \sim 17$ are almost completely damped. However, for the well-resolved frequencies ($k < 8$), the RMSE is lower in presence of the background.

For linear finite difference schemes, amplification factors above one imply instability. For the Galperin scheme, the amplification factors for a single timestep fluctuate depending on the centres of mass, but the solution remains bounded due to non-negativity and conservation of mass. Based on numerical tests, the asymptotic solution as $t \to \infty$ in a periodic domain is either a constant, or a combination

of rectangular pulses. These cases correspond to the dissipative or non-dissipative behaviour depicted in Fig. 9.

The switch between the dissipative or non-dissipative domains is explained by variation of the centres of mass. Presence of a background constrains the range of variation of the centres of mass, since the changes in centre of mass depend on the relative magnitude of the perturbation that enters the gridcell from upwind side. Paper IV discusses use of a "smoothing factor" which essentially fixes the scheme to the dissipative domain. However, a better solution might be achieved by modifying the reconstruction function (Eq. 12). Since the publication of Paper IV, further research (R. Kouznetsov, personal communication) has shown that by allowing the reconstruction function to depend also on the values of the adjacent grid cells, it is possible to devise a piecewise constant reconstruction function which is invariant under addition of constant. Alternatively, a higher order scheme can be constructed using a piecewise linear reconstruction function.

6 Conclusions and future work

This study has presented applications of variational assimilation methods in air quality forecasting and volcanic source term inversion problems. Furthermore, a numerical scheme for solving the advection equation has been evaluated using recently published benchmarks.

The impact of conventional data assimilation, where observations are used to adjust the initial condition of a forecast, was evaluated for regional-scale predictions of NO_2, SO_2 and ozone. In Paper II, the forecast correlation and bias were found to improve for up to 12-24 hours for ozone, but for only 6-12 hours for NO_2. The impact on SO_2 forecasts was evaluated in a separate study (Paper I), where the improvement in RMSE extended for about 12 hours. Thus, especially for short-lived pollutants, this type of data assimilation has limited use in forecasting.

For SO_2, the conventional data assimilation approach was compared to a scheme similar to that presented by Elbern et al. (2007), where emission fluxes are adjusted along with the initial conditions. This setup was found to produce forecast improvements which were more persistent, but on average, small. Significant improvements could be obtained for stations where the emission adjustments persisted over the two-week experiment. This suggests that the emission adjustment can be effective assimilation strategy, if the forecast skill is affected by strong and systematic biases in the emission forcing.

For O_3 and NO_2, the analysis scores were substantially improved by iterative refining of the background and observation error standard deviations. The final values for observation errors are larger than commonly assumed, but similar to a previous study (Gaubert et al., 2014) applying a similar estimation procedure. Better quantification of the representativeness errors of air quality monitoring data would be valuable for both data assimilation and model evaluation based on such data.

In Paper III, the 4D-Var method was adapted for solving the inverse problem of reconstructing the vertical and temporal profile of volcanic SO_2 emissions. The 4D-Var based inversion regularised by truncated iteration was shown to produce equivalent results to the more common direct method with Tikhonov regularisation. Depending on the setup, the variational method may require considerably less computation.

The SO_2 retrievals from the IASI instrument were assimilated using the 4D-Var inversion scheme. Including the IASI plume height retrievals in the inversion in addition to the column density retrievals, reduced the emissions above 10-12 km. The resulting vertical distribution is more consistent with radar observations of the plume, which supports the conclusion that the SO_2 emissions of Eyjafjallajökull were, similarly to ash, confined to the troposphere.

The inverse modelling is established by several studies as a means for incorporating observations into simulations of volcanic plumes. The same approach might turn out useful for simulating other intermittent emissions sources, such as wind blown dust and wildfires. However, the difficulty of accommodating realistic model errors is a weakness of the current inversion approach, and improving this aspect may require significant algorithmic changes.

Evaluation of the advection scheme presented by Galperin (1999) indicated that the scheme is generally comparable in accuracy to the schemes evaluated by Lauritzen et al. (2014), with rate of convergence slightly lower than second order. The scheme is conservative and preserves non-negativity of the tracers, but was found to have a strongly nonlinear response under addition of a constant.

For a single tracer, the scheme was found to have good computational performance compared the schemes described by Kaas et al. (2013). However, the lack of common benchmarks makes comparing the numerical performance across schemes difficult. A uniform, transparent methodology for assessing the computational aspects of numerical schemes would be helpful for potential users of the numerical schemes.

References

Arason, P., Petersen, G. N., and Bjornsson, H. (2011). Observations of the altitude of the volcanic plume during the eruption of Eyjafjallajökull, April–May 2010. *Earth System Science Data*, 3:9–17.

Benedetti, A., Morcrette, J.-J., Boucher, O., Dethof, A., Engelen, R. J., Fisher, M., Flentje, H., Huneeus, N., Jones, L., Kaiser, J. W., Kinne, S., Mangold, A., Razinger, M., Simmons, A. J., and Suttie, M. (2009). Aerosol analysis and forecast in the European Centre for Medium-Range Weather Forecasts Integrated Forecast System: 2. Data assimilation. *Journal of Geophysical Research*, 114(D13205).

Blond, N. and Vautard, R. (2004). Three-dimensional ozone analyses and their use for short-term ozone forecasts. *Journal of Geophysical Research*, 109(D17303).

Bocquet, M. (2007). High-resolution reconstruction of a tracer dispersion event: application to ETEX. *Quarterly Journal of the Royal Meteorological Society*, 133:1013–1026.

Boichu, M., Menut, L., Khvorostyanov, D., Clarisse, L., Clerbaux, C., Turquety, S., and Coheur, P.-F. (2013). Inverting for volcanic SO2 flux at high temporal resolution using spaceborne plume imagery and chemistry-transport modelling: the 2010 Eyjafjallajökull eruption case study. *Atmospheric Chemistry and Physics*, 13:8569–8584.

Bott, A. (1989). A positive definite advection scheme obtained by nonlinear renormalization of the advective fluxes. *Monthly Weather Review*, 117(5):1006–1016.

Byrd, R., Lu, P., Nocedal, J., and Zhu, C. (1995). A limited memory algorithm for bound constrained optimization. *SIAM Journal on Scientific Computing*, 16(5):1190–1208.

Carboni, E., Grainger, R., Walker, J., Dudhia, A., and Siddans, R. (2012). A new scheme for sulphur dioxide retrieval from IASI measurements: application to the Eyjafjallajökull eruption of April and May 2010. *Atmospheric Chemistry and Physics*, 12(23):11417–11434.

Clerbaux, C., Boynard, A., Clarisse, L., George, M., Hadji-Lazaro, J., Herbin, H., Hurtmans, D., Pommier, M., Razavi, A., Turquety, S., Wespes, C., and Coheur, P.-F. (2009). Monitoring of atmospheric composition using the thermal infrared IASI/MetOp sounder. *Atmospheric Chemistry and Physics*, 9(16):6041–6054.

Colella, P. and Woodward, P. (1984). The piecewise parabolic method (PPM) for gas-dynamical simulations. *Journal of computational physics*, 54(1):174–201.

Collins, W. D., Rasch, P. J., Eaton, B. E., Khattatov, B. V., and Zender, S. (2001). Simulating aerosols using a chemical transport model with assimilation of satellite aerosol retrievals: Methodology for INDOEX. *Journal of Geophysical Research*, 106:7313–7336.

Curier, R., Timmermans, R., Calabretta-Jongen, S., Eskes, H., Segers, A., Swart, D., and Schaap, M. (2012). Improving ozone forecasts over Europe by synergistic use of the LOTOS-EUROS chemical transport model and in-situ measurements. *Atmospheric Environment*, 60:217–226.

Davoine, X. and Bocquet, M. (2007). Inverse modelling-based reconstruction of the Chernobyl source term available for long-range transport. *Atmospheric Chemistry and Physics*, 7(6):1549–1564.

Dee, D. P., Uppala, S. M., Simmons, A. J., Berrisford, P., Poli, P., Kobayashi, S., Andrae, U., Balmaseda, M. A., Balsamo, G., Bauer, P., Bechtold, P., Beljaars, A. C. M., Berg, L. V. D., Bidlot, J., Bormann, N., Delsol, C., Dragani, R., Fuentes, M., Geer, A. J., Haimberger, L., Healy, S. B., Hersbach, H., Hólm, E. V., Isaksen, L., Kållberg, P., Köhler, M., Matricardi, M., McNally, A. P., Monge-Sanz, B. M., Morcrette, J.-J., Park, B.-K., Peubey, C., de Rosnay, P., Tavolato, C., Thépaut, J.-N., and Vitart, F. (2011). The ERA-Interim reanalysis : configuration and performance of the data assimilation system. *Quarterly Journal of the Royal Meteorological Society*, 137(April):553–597.

Derber, J. C. (1989). A Variational Continuous Assimilation Technique. *Monthly Weather Review*, 117(11):2437–2446.

Desroziers, G., Berre, L., Chapnik, B., and Poli, P. (2005). Diagnosis of observation, background and analysis-error statistics in observation space. *Quarterly Journal of the Royal Meteorological Society*, 131(613):3385–3396.

Eckhardt, S., Prata, A. J., Seibert, P., Stebel, K., and Stohl, A. (2008). Estimation of the vertical profile of sulfur dioxide injection into the atmosphere by a volcanic eruption using satellite column measurements and inverse transport modeling. *Atmospheric Chemistry and Physics*, 8:3881–3897.

Egan, B. and Mahoney, J. (1972). Numerical Modeling of Advection and Diffusion of Urban Area Source Pollutants. *Journal of Applied Meteorology*, 11:312–322.

Elbern, H. and Schmidt, H. (1999). A four-dimensional variational chemistry data assimilation scheme for Eulerian chemistry transport modeling. *Journal of Geophysical Research*, 104(D15):18583–18598.

Elbern, H. and Schmidt, H. (2001). Ozone episode analysis by four-dimensional variational chemistry data assimilation. *Journal of Geophysical Research*, 106(D4):3569–3590.

Elbern, H., Schmidt, H., and Ebel, A. (1997). Variational data assimilation for tropospheric chemistry modeling. *Journal of Geophysical Research*, 102(D13):15967–15985.

Elbern, H., Schmidt, H., Talagrand, O., and Ebel, A. (2000). 4D-variational data assimilation with an adjoint air quality model for emission analysis. *Environmental Modelling & Software*, 15(6-7):539–548.

Elbern, H., Strunk, A., Schmidt, H., and Talagrand, O. (2007). Emission rate and chemical state estimation by 4-dimensional variational inversion. *Atmospheric Chemistry and Physics*, 7:3749–3769.

Enting, I. G. (2002). *Inverse Problems in Atmospheric Constituent Transport*. Cambridge University Press.

Enting, I. G. and Mansbridge, J. V. (1989). Seasonal sources and sinks of atmospheric CO2 Direct inversion of filtered data. *Tellus B*, 41B(2):111–126.

Evensen, G. (1994). Sequential data assimilation with a nonlinear quasi-geostrophic model using Monte Carlo methods to forecast error statistics. *Journal of Geophysical Research*, 99(C5):10143–10162.

Evensen, G. (2003). The Ensemble Kalman Filter: theoretical formulation and practical implementation. *Ocean Dynamics*, 53(4):343–367.

Fisher, M. and Lary, D. J. (1995). Lagrangian four-dimensional variational data assimilation of chemical species. *Quarterly Journal of the Royal Meteorological Society*, 121(527):1681–1704.

Fleming, H. (1990). Equivalence of regularization and truncated iteration in the solution of ill-posed image reconstruction problems. *Linear Algebra and its Applications*, 130:133–150.

Flemming, J. and Inness, A. (2013). Volcanic sulfur dioxide plume forecasts based on UV-satellite retrievals for the 2011 Grímsvötn and the 2010 Eyjafjallajökull eruption. *Journal of Geophysical Research: Atmospheres*, 118(May 2010).

Galperin, M. (2000). The approaches to correct computation of airborne pollution advection. In *Problems of Ecological Monitoring and Ecosystem Modelling. XVII (in Russian)*, pages 54–68. Gidrometeoizdat.

Galperin, M. V. (1999). Approaches for improving the numerical solution of the advection equation. In Zlatev, Z., editor, *Large-Scale Computations in Air Pollution Modelling, Proc. NATO Advanced Research Workshop on Large Scale Computations in Air Pollution Modelling, Sofia, Bistritza*, pages 161–172, Sofia. Kluwer Academic Publishers, Dordrecht, The Netherlands.

Gaubert, B., Coman, A., Foret, G., Meleux, F., Ung, A., Rouil, L., Ionescu, A., Candau, Y., and Beekmann, M. (2014). Regional scale ozone data assimilation using an ensemble Kalman filter and the CHIMERE chemical transport model. *Geoscience Model Development*, 7:283–302.

Gery, M., Whitten, G., Killus, J., and Dodge, M. (1989). A photochemical kinetics mechanism for urban and regional scale computer modeling. *Journal of Geophysical Research*, 94(D10):12925–12956.

Giering, R. and Kaminski, T. (1998). Recipes for adjoint code construction. *ACM Transactions on Mathematical Software*, 24(4):437–474.

Gilbert, J. C. and Lemaréchal, C. (1989). Some numerical experiments with variable-storage quasi-Newton algorithms. *Mathematical Programming*, 45:407–435.

Godunov, S. K. (1959). Finite difference methods for numerical computation of discontinuous solutions of equations of fluid dynamics. *Mat. Sb.*, 47:271–295.

Gou, T. and Sandu, A. (2011). Continuous versus discrete advection adjoints in chemical data assimilation with CMAQ. *Atmospheric Environment*, 45(28):4868–4881.

Hakami, A., Henze, D. K., Seinfeld, J. H., Singh, K., Sandu, A., Kim, S., and Li, Q. (2007). The Adjoint of CMAQ. *Environmental Science & Technology*, 41(22):7807–7817.

Hansen, P. C. (1992). Analysis of Discrete Ill-Posed Problems by Means of the L-Curve. *SIAM Review*, 34(4):561–580.

Heng, Y., Hoffmann, L., Griessbach, S., Rößler, T., and Stein, O. (2016). Inverse transport modeling of volcanic sulfur dioxide emissions using large-scale simulations. *Geoscientific Model Development*, 9:1627–1645.

Henne, S., Brunner, D., Folini, D., Solberg, S., Klausen, J., and Buchmann, B. (2010). Assessment of parameters describing representativeness of air quality in-situ measurement sites. *Atmospheric Chemistry and Physics*, 10:3561–3581.

Henze, D., Hakami, A., and Seinfeld, J. (2007). Development of the adjoint of GEOS-Chem. *Atmospheric Chemistry & Physics*, 7:2413–2433.

Houweling, S., Kaminski, T., Dentener, F., Lelieveld, J., and Heimann, M. (1999). Inverse modeling of methane sources and sinks using the adjoint of a global transport model. *Journal of Geophysical Research*, 104(D21):26137–26160.

Inness, A., Baier, F., Benedetti, A., Bouarar, I., Chabrillat, S., Clark, H., Clerbaux, C., Coheur, P., Engelen, R. J., Errera, Q., Flemming, J., George, M., Granier, C., Hadji-Lazaro, J., Huijnen, V., Hurtmans, D., Jones, L., Kaiser, J. W., Kapsomenakis, J., Lefever, K., Leitão, J., Razinger, M., Richter, A., Schultz, M. G., Simmons, A. J., Suttie, M., Stein, O., Thépaut, J.-N., Thouret, V., Vrekoussis, M., and Zerefos, C. (2013). The MACC reanalysis: an 8 yr data set of atmospheric composition. *Atmospheric Chemistry and Physics*, 13(8):4073–4109.

Issartel, J.-P. and Baverel, J. (2003). Inverse transport for the verification of the Comprehensive Nuclear Test Ban Treaty. *Atmospheric Chemistry and Physics*, 3(3):475–486.

Joly, M. and Peuch, V.-H. (2012). Objective classification of air quality monitoring sites over Europe. *Atmospheric Environment*, 47:111–123.

Kaas, E., Sørensen, B., Lauritzen, P. H., and Hansen, A. B. (2013). A hybrid Eulerian–Lagrangian numerical scheme for solving prognostic equations in fluid dynamics. *Geoscientific Model Development*, 6(6):2023–2047.

Kaminski, T., Heimann, M., and Giering, R. (1999). A coarse grid three-dimensional global inverse model of the atmospheric transport 2. Inversion of the transport of CO2 in the 1980s. *Journal of Geophysical Research*, 104(D15):18555–18581.

Koohkan, M. R. and Bocquet, M. (2012). Accounting for representativeness errors in the inversion of atmospheric constituent emissions : application to the retrieval of regional carbon monoxide fluxes. *Tellus B*, 64(19047).

Kouznetsov, R. and Sofiev, M. (2012). A methodology for evaluation of vertical dispersion and dry deposition of atmospheric aerosols. *Journal of Geophysical Research*, 117(D1):1–19.

Kristiansen, N., Arnold, D., Maurer, C., Vira, J., Radulescu, R., Martin, D., Stohl, A., Stebel, K., Sofiev, M., O'Dowd, C., and Wotawa, G. (2017). Improving model simulations of volcanic emission clouds and assessing model uncertainties. In Riley, K., Webley, P., and Thompson, M., editors, *Natural Hazard Uncertainty Assessment: Modeling and Decision Support*, AGU Geophysical Monograph Series. American Geophysical Union.

Kristiansen, N. I., Stohl, A., Prata, A. J., Richter, A., Eckhardt, S., Seibert, P., Hoffmann, A., Ritter, C., Bitar, L., Duck, T. J., and Stebel, K. (2010). Remote sensing and inverse transport modeling of the Kasatochi eruption sulfur dioxide cloud. *Journal of Geophysical Research*, 115:1–18.

Kuenen, J. J. P., Visschedijk, A. J. H., Jozwicka, M., and Denier van der Gon, H. A. C. (2014). TNO-MACC_II emission inventory: a multi-year (2003–2009) consistent high-resolution European emission inventory for air quality modelling. *Atmospheric Chemistry and Physics*, 14:10963–10976.

Kukkonen, J., Olsson, T., Schultz, D. M., Baklanov, A., Klein, T., Miranda, A., Monteiro, A., Hirtl, M., Tarvainen, V., Boy, M., Peuch, V.-H., Poupkou, A., Kioutsioukis, I., Finardi, S., Sofiev, M., Sokhi, R., Lehtinen, K. E. J., Karatzas, K., San José, R., Astitha, M., Kallos, G., Schaap, M., Reimer, E., Jakobs, H., and Eben, K. (2012). A review of operational, regional-scale, chemical weather forecasting models in Europe. *Atmospheric Chemistry and Physics*, 12(1):1–87.

Lanser, D. (1999). Analysis of operator splitting for advection–diffusion–reaction problems from air pollution modelling. *Journal of Computational and Applied Mathematics*, 111(1-2):201–216.

Lauritzen, P., Ullrich, P., and Nair, R. (2011). Atmospheric Transport Schemes: Desirable Properties and a Semi-Lagrangian View on Finite-Volume Discretizations. In Lauritzen, P., Jablonowski, C., Taylor, M., and Nair, R., editors, *Numerical Techniques for Global Atmospheric Models*, volume 80 of *Lecture Notes in Computational Science and Engineering*, pages 185–250. Springer Berlin Heidelberg.

Lauritzen, P. H., Nair, R. D., and Ullrich, P. A. (2010). A conservative semi-Lagrangian multi-tracer transport scheme (CSLAM) on the cubed-sphere grid. *Journal of Computational Physics*, 229(5):1401–1424.

Lauritzen, P. H., Skamarock, W. C., Prather, M. J., and Taylor, M. A. (2012). A standard test case suite for two-dimensional linear transport on the sphere. *Geoscientific Model Development*, 5(3):887–901.

Lauritzen, P. H., Ullrich, P. A., Jablonowski, C., Bosler, P. A., Calhoun, D., Conley, A. J., Enomoto, T., Dong, L., Dubey, S., Guba, O., Hansen, A. B., Kaas, E., Kent, J., Lamarque, J.-F., Prather, M. J., Reinert, D., Shashkin, V. V., Skamarock, W. C., Sørensen, B., Taylor, M. A., and Tolstykh, M. A. (2014). A standard test case suite for two-dimensional linear transport on the sphere: results from a collection of state-of-the-art schemes. *Geoscientific Model Development*, 7(1):105–145.

Le Dimet, F.-X. and Talagrand, O. (1986). Variational algorithms for analysis and assimilation of meteorological observations: theoretical aspects. *Tellus A*, 38A(2):97–110.

LeVeque, R. J. (1992). *Numerical Methods for Conservation Laws*. Birkhäuser Basel, 2 edition.

Lin, S.-J. and Rood, R. B. (1997). An explicit flux-form semi-Lagrangian shallow-water model of the sphere. *Quarterly Journal of Royal Meteorological Society*, 123:2477–2498.

Lorenc, A. C. (1986). Analysis methods for numerical weather prediction. *Quarterly Journal of the Royal Meteorological Society*, 112(474):1177–1194.

Lorenz, E. N. (1963). Deterministic Nonperiodic Flow. *Journal of the Atmospheric Sciences*, 20(2):130–141.

Lorenz, E. N. (1982). Atmospheric predictability experiments with a large numerical model. *Tellus A*, 34:505–513.

Magnusson, L. and Källén, E. (2013). Factors influencing skill improvements in the ECMWF forecasting system. *Monthly Weather Review*, 141(9):3142–3153.

Marchuk, G. (1995). *Adjoint equations and analysis of complex systems*. Kluwer Academic Publishers, Dordrecht, The Netherlands.

Ménard, R. (2016). Error covariance estimation methods based on analysis residuals: Theoretical foundation and convergence properties derived from simplified observation networks. *Quarterly Journal of the Royal Meteorological Society*, 142(694):257–273.

Miyazaki, K., Eskes, H. J., and Sudo, K. (2012). Global NOx emission estimates derived from an assimilation of OMI tropospheric NO 2 columns. *Atmospheric Chemistry and Physics*, 12(2):2263–2288.

Moxnes, E. D., Kristiansen, N. I., Stohl, A., Clarisse, L., Durant, A., Weber, K., and Vogel, A. (2014). Separation of ash and sulfur dioxide during the 2011 Grimsvötn eruption. *Journal of Geophysical Research*, 119:7477–7501.

Müller, J. F. and Stavrakou, T. (2005). Inversion of CO and NOx emissions using the adjoint of the IMAGES model. *Atmospheric Chemistry and Physics*, 5:1157–1186.

Nair, R. D. and Machenhauer, B. (2002). The Mass-Conservative Cell-Integrated Semi-Lagrangian Advection Scheme on the Sphere. *Monthly Weather Review*, 130(3):649–667.

Pagowski, M., Grell, G. A., McKeen, S. A., Peckham, S. E., and Devenyi, D. (2010). Three-dimensional variational data assimilation of ozone and fine particulate matter observations: some results using the Weather Research and Forecasting-Chemistry model and Grid-point Statistical Interpolation. *Quarterly Journal of the Royal Meteorological Society*, 136(653):2013–2024.

Peters, W., Krol, M. C., van der Werf, G. R., Houweling, S., Jones, C. D., Hughes, J., Schaefer, K., Masarie, K. A., Jacobson, A. R., Miller, J. B., Cho, C. H., Ramonet, M., Schmidt, M., Ciattaglia, L., Apadula, F., Heltai, D., Meinhardt, F., di Sarra, A. G., Piacentino, S., Sferlazzo, D., Aalto, T., Hatakka, J., Ström, J., Haszpra, L., Meijer, H. A. J., van Der Laan, S., Neubert, R. E. M., Jordan, A., Rodó, X., Morguí, J. A., Vermeulen, A. T., Popa, E., Rozanski, K., Zimnoch, M., Manning, A. C., Leuenberger, M., Uglietti, C., Dolman, A. J., Ciais, P., Heimann, M., and Tans, P. (2010). Seven years of recent European net terrestrial carbon dioxide exchange constrained by atmospheric observations. *Global Change Biology*, 16(4):1317–1337.

Petrova, S., Kirova, H., Syrakov, D., and Prodanova, M. (2008). Some fast variants of TRAP scheme for solving advection equation — comparison with other schemes. *Computers & Mathematics with Applications*, 55(10):2363–2380.

Peylin, P., Law, R. M., Gurney, K. R., Chevallier, F., Jacobson, A. R., Maki, T., Niwa, Y., Patra, P. K., Peters, W., Rayner, P. J., Rödenbeck, C., Van Der Laan-Luijkx, I. T., and Zhang, X. (2013). Global atmospheric carbon budget: Results from an ensemble of atmospheric CO2 inversions. *Biogeosciences*, 10(10):6699–6720.

Poupkou, A., Giannaros, T., Markakis, K., Kioutsioukis, I., Curci, G., Melas, D., and Zerefos, C. (2010). A model for European Biogenic Volatile Organic Compound emissions: Software development and first validation. *Environmental Modelling & Software*, 25(12):1845–1856.

Prather, M. (1986). Numerical Advection by Conservation of Second-Order Moments. *J. Geophys. Res*, 91(D6):6671–6681.

Pudykiewicz, J. (1998). Application of adjoint tracer transport equations for evaluating source parameters. *Atmospheric environment*, 32(17):3039–3050.

Robertson, L. and Persson, C. (1993). Attempts to apply four dimensional data assimilation of radiological data using the adjoint technique. *Radiation protection dosimetry*, 50(2-4):333–337.

Rood, R. (1987). Numerical advection algorithms and their role in atmospheric transport and chemistry models. *Reviews of geophysics*, 25(1):71–100.

Russell, G. and Lerner, J. (1981). A new finite-differencing scheme for the tracer transport equation. *Journal of Applied Meteorology*, 20:1483–1498.

Sandu, A. and Sander, R. (2006). Technical note: Simulating chemical systems in Fortran90 and Matlab with the Kinetic PreProcessor KPP-2.1. *Atmospheric Chemistry and Physics*, 6(1):187–195.

Santillana, M., Zhang, L., and Yantosca, R. (2016). Estimating numerical errors due to operator splitting in global atmospheric chemistry models: Transport and chemistry. *Journal of Computational Physics*, 305:372–386.

Santos, R. J. (1996). Equivalence of regularization and truncated iteration for general ill-posed problems. *Linear algebra and its applications*, 236:25–33.

Schutgens, N. A. J., Gryspeerdt, E., Weigum, N., Tsyro, S., Goto, D., Schulz, M., and Stier, P. (2016). Will a perfect model agree with perfect observations? The impact of spatial sampling. *Atmospheric Chemistry and Physics*, 16:6335–6353.

Shankar Rao, K. (2007). Source estimation methods for atmospheric dispersion. *Atmospheric Environment*, 41(33):6964–6973.

Silver, J. D., Brandt, J., Hvidberg, M., Frydendall, J., and Christensen, J. H. (2013). Assimilation of OMI NO2 retrievals into the limited-area chemistry-transport model DEHM (V2009.0) with a 3-D OI algorithm. *Geoscientific Model Development*, 6(1):1–16.

Singh, K., Jardak, M., Sandu, A., Bowman, K., Lee, M., and Jones, D. (2011). Construction of non-diagonal background error covariance matrices for global chemical data assimilation. *Geoscientific Model Development*, 4(2):299–316.

Sofiev, M. (2000). A model for the evaluation of long-term airborne pollution transport at regional and continental scales. *Atmospheric Environment*, 34(15):2481–2493.

Sofiev, M. (2002). Extended resistance analogy for construction of the vertical diffusion scheme for dispersion models. *Journal of Geophysical Research*, 107(D12):ACH 10–1 – ACH 10–8.

Sofiev, M., Galperin, M., and Genikhovich, E. (2008). A construction and Evaluation of Eulerian Dynamic Core for the Air Quality and Emergency Modelling System SILAM. In Borrego, C. and Miranda, A. I., editors, *Air Pollution Modeling and Its Application XIX*, number 2004 in NATO Science for Peace and Security Series C: Environmental Security, pages 699–701. Springer.

Sofiev, M., Siljamo, P., Valkama, I., Ilvonen, M., and Kukkonen, J. (2006). A dispersion modelling system SILAM and its evaluation against ETEX data. *Atmospheric Environment*, 40(4):674–685.

Sportisse, B. (2000). An Analysis of Operator Splitting Techniques in the Stiff Case. *Journal of Computational Physics*, 161:140–168.

Staniforth, A. and Côte, J. (1991). Semi-Lagrangian integration schemes for atmospheric models - a review. *Monthly Weather Review*, 119:2206–2223.

Stohl, A., Prata, A. J., Eckhardt, S., Clarisse, L., Durant, A., Henne, S., Kristiansen, N. I., Minikin, A., Schumann, U., Seibert, P., Stebel, K., Thomas, H. E., Thorsteinsson, T., Tørseth, K., and Weinzierl, B. (2011). Determination of time- and height-resolved volcanic ash emissions and their use for quantitative ash dispersion modeling: the 2010 Eyjafjallajökull eruption. *Atmospheric Chemistry and Physics*, 11(9):4333–4351.

Talagrand, O. (1997). Assimilation of observations, an introduction. *Journal of the Meteorological Society of Japan*, 75(1B):191–209.

Tarantola, A. (2005). *Inverse problem theory and methods for model parameter estimation*. Society of Industrial and Applied Mathematics.

Tombette, M., Mallet, V., and Sportisse, B. (2009). PM 10 data assimilation over Europe with the optimal interpolation method. *Atmospheric Chemistry and Physics*, 9(1):57–70.

Trémolet, Y. (2006). Accounting for an imperfect model in 4D-Var. *Quarterly Journal of the Royal Meteorological Society*, 132(621):2483–2504.

van Loon, M., Builtjes, P., and Segers, A. J. (2000). Data assimilation of ozone in the atmospheric transport chemistry model LOTOS. *Environmental Modelling & Software*, 15:603–609.

Wang, X., Mallet, V., Berroir, J.-p., and Herlin, I. (2011). Assimilation of OMI NO2 retrievals into a regional chemistry-transport model for improving air quality forecasts over Europe. *Atmospheric Environment*, 45(2):485–492.

Weaver, C., da Silva, A., Chin, M., Ginoux, P., Dubovik, O., Flittner, D., Zia, A., Remer, L., Holben, B., and Gregg, W. (2007). Direct Insertion of MODIS Radiances in a Global Aerosol Transport Model. *Journal of the Atmospheric Sciences*, 64:808–827.

Wu, L., Mallet, V., Bocquet, M., and Sportisse, B. (2008). A comparison study of data assimilation algorithms for ozone forecasts. *Journal of Geophysical Research*, 113(D20310).

Zhang, J., Reid, J. S., Westphal, D. L., Baker, N. L., and Hyer, E. J. (2008). A system for operational aerosol optical depth data assimilation over global oceans. *Journal of Geophysical Research*, 113(D10208).

Zidikheri, M. J. and Potts, R. J. (2015). A simple inversion method for determining optimal dispersion model parameters from satellite detections of volcanic sulfur dioxide. *Journal of Geophysical Research: Atmospheres*, 120.